Crystal-structure units of the *R* (Fe_3Mo_2) phase in the Fe-Mo alloy system

Toshihiro Doi,[1] Makoto Tanimura,[2] and Yasumasa Koyama[1]
[1]*Department of Electronic and Photonic Systems and Kagami Memorial Laboratory for Materials Science and Technology, Waseda University, Shinjuku, Tokyo 169-8555, Japan*
[2]*Research Department, NISSAN ARC, Limited, Yokosuka, Kanagawa 237-0061, Japan*
(Received 2 December 2007; published 18 April 2008)

Around 37 at. % Mo in the Fe-Mo alloy system, in the temperature range between 1473 and 1761 K, there exists the intermetallic-compound *R* phase, whose crystal structure involves 12-, 14-, 15-, and 16-coordination polyhedra. To determine the crystal-structure units of the *R* phase, the crystallographic features of the bcc-to-*R* structural change in the (bcc→bcc+*R*) reaction of the Fe-Mo system have been investigated by transmission electron microscopy. It was found that atomic columns, which were identified as the secondary structural unit, appeared first in the initial stage of the reaction. Based on this fact, the *R* phase is understood to have a crystal structure consisting of atomic columns, just as in the case of the μ structure [A. Hirata *et al.*, Phys. Rev. B **74**, 054204 (2006)]. Although only 12-coordination polyhedra form an atomic column in the μ structure, the column in the *R* structure consists of two kinds of polyhedra: that is, 16- and 12-coordination ones. Of these two polyhedra, in particular, the appearance of a 16-coordination polyhedron as the primary structural unit of the *R* structure is associated with the formation of covalent bonds in alloys.

DOI: 10.1103/PhysRevB.77.134205 PACS number(s): 61.66.Dk, 71.20.Lp, 71.20.Be, 68.37.Lp

I. INTRODUCTION

It is known that there exist intermetallic-compound phases with their crystal structures consisting of complex coordination polyhedra.[1–5] In addition to the Laves and μ phases,[6,7] for example, the so-called *R* phase was found around the Fe_3Mo_2 composition in the Fe-Mo alloy system.[8] The feature of the crystal structure of this phase, which is called the *R* structure, is that 12-, 14-, 15-, and 16-coordination (CN) polyhedra are involved in the structure, as in the case of the μ phase. Although structural data for the *R* structure with rhombohedral symmetry have been established for the Mn-Si and Mo-Co-Cr alloy systems,[9,10] its characteristic features, such as the structural units, are not yet understood. The simple question remains whether these polyhedra can be identified as structural units or not in the *R* structure. In order to obtain the answer, we have investigated the formation process of the *R* structure from the bcc structure. We believe that true structural units should appear first during the formation of the *R* structure. As a matter of fact, our previous study on the formation of the μ structure revealed that the secondary structural unit of the μ structure was a decagonal atomic column, which was characterized by a one-dimensional array of CN12 polyhedra as the primary structural unit. In other words, it is understood that the μ structure is one of the crystal structures consisting of atomic columns in transition-metal alloys.[11]

The *R* phase in the Fe-Mo alloy system is present in the temperature range between 1473 and 1761 K around 37 at. % Mo.[8] According to the reported Fe-Mo phase diagram,[12] the (bcc→bcc+*R*) reaction is expected to occur by maintaining the metastable-bcc alloy, with a composition near 20 at. % Mo, in the above temperature range. Although detailed structural data for the *R* structure have not been obtained for the Fe-Mo alloy system, we can examine the crystallographic features of the bcc-to-*R* structural change during the (bcc→bcc+*R*) reaction. As the structural units of the *R* structure should appear first in the structural change, the presence of this reaction is the reason why we focused on the Fe-Mo alloy system, in addition to the previous accumulation of our experimental data on the μ-structure formation in this system.[11] Metastable-bcc 18 at. % Mo alloy samples were annealed at 1523 K to initiate the (bcc→bcc+*R*) reaction, and the crystallographic features of the annealed samples were then examined by transmission electron microscopy. Based on the present experimental data for the Fe-Mo alloy system, together with the reported structural data of the *R* structure for the Mo-Co-Cr system,[10] we identify the crystal-structure units of the *R* structure and propose an atomic-displacement model for the structural-unit formation from the bcc structure. The physical origin of the formation of the primary structural unit in the *R* structure is also discussed on the basis of the proposed atomic-displacement model.

II. EXPERIMENTAL PROCEDURE

In this study, we used Fe-18 at. % Mo alloy samples to examine the crystallographic features of the bcc-to-*R* structural change, in addition to those of the *R* structure itself. Ingots of the alloy were prepared from Fe and Mo with purity of 99.9% by an Ar-arc-melting technique. They were kept at 1673 K for 24 h in the bcc single phase, followed by quenching into ice water, for solution treatment. To stimulate the (bcc→bcc+*R*) reaction, metastable-bcc samples cut from these ingots were annealed at 1523 K for various annealing times. The crystallographic features of these samples were examined by a 3010-type transmission electron microscope with an accelerating voltage of 300 kV. Thin specimens for transmission-electron-microscope observation were prepared by an Ar-ion thinning method.

III. EXPERIMENTAL RESULTS

The experimental data revealed that a (bcc+*R*) coexistence state was present in samples annealed for more than

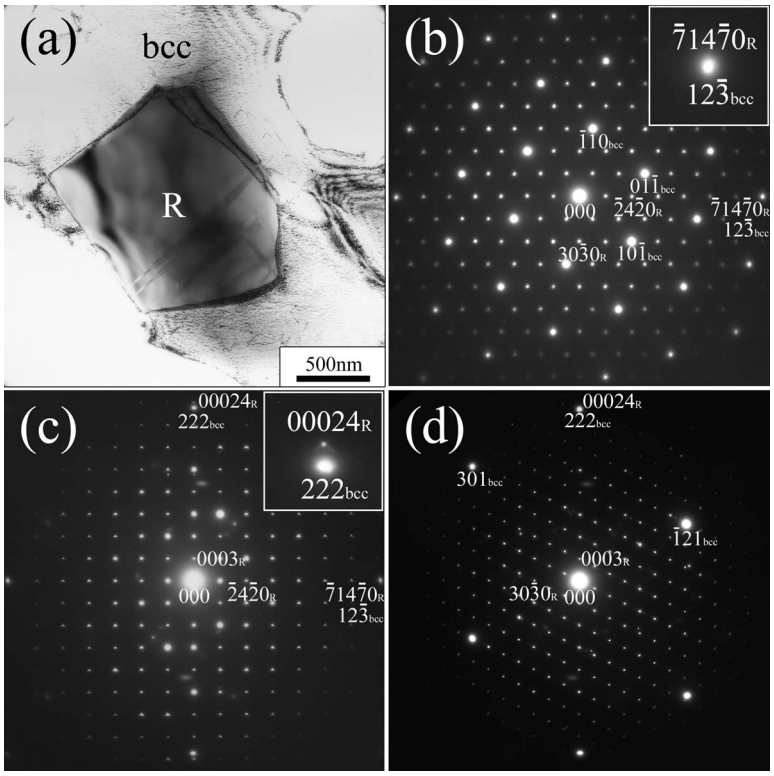

FIG. 1. (a) Bright field image of a Fe-18 at. % Mo alloy sample annealed at 1523 K for 24 h, together with three corresponding electron diffraction patterns in (b), (c), and (d). The electron beam incidences of the patterns in (b), (c), and (d) are, respectively, parallel to the $[111]_{bcc}$, $[5\bar{4}\bar{1}]_{bcc}$, and $[12\bar{3}]_{bcc}$ directions. The insets in (b) and (c) also show enlarged patterns around the $12\bar{3}_{bcc}$ reflection and around the 222_{bcc} reflection, respectively. In the patterns, it is found that the $[0001]_R$ electron incidence is parallel to the $[111]_{bcc}$ incidence and that the position of the $\bar{7}14\bar{7}0_R$ reflection is, for instance, identical to that of $12\bar{3}_{bcc}$, where the subscript R denotes the R structure. These findings are clear evidence for the orientation relationship of $[111]_{bcc}\|[0001]_R$ and $(12\bar{3})_{bcc}\|(\bar{7}14\bar{7}0)_R$.

1 min. The striking feature of the (bcc $\rightarrow$ bcc+R) reaction is that, in samples annealed for 1 and 3 min, there existed transitional states between the bcc and R states. It was also found that these transitional states could be classified into two groups: that is, initial and intermediate states. Before describing the detailed features of these two transitional states, we first report the crystallographic features of equilibrium-state samples, which were obtained by annealing metastable-bcc samples for 24 h.

Figure 1 shows both a bright field image and three corresponding electron diffraction patterns of an equilibrium-state sample annealed for 24 h. The electron incidences of the patterns in (b), (c), and (d) are, respectively, parallel to the $[111]_{bcc}$, $[5\bar{4}\bar{1}]_{bcc}$, and $[12\bar{3}]_{bcc}$ directions in terms of a cubic notation, while the image in (a) was taken for the $[111]_{bcc}$ incidence. In the image, an R precipitate observed as dark contrast is present in the bright contrast bcc matrix. The size of the precipitate is estimated to be about 1 μm. Strong and weak reflections in the diffraction patterns were confirmed to be, respectively, due to the bcc and R structures. The orientation relationship between the bcc and R structures was then determined by using electron diffraction patterns with different incidences, including the patterns in (a), (b), and (c). As a result of the careful analysis of the diffraction patterns, we found only one relationship: that is, $[111]_{bcc}\|[0001]_R$ and $(12\bar{3})_{bcc}\|(\bar{7}14\bar{7}0)_R$, where the crystallographic direction and plane of the R structure are indexed in terms of a hexagonal notation. It should be remarked that Donnadieu and Redjaimia already obtained the same orientation relationship for the Fe-Cr-Ni-Mo-C alloy system.[13]

Keeping the above relationship in mind, we took high-resolution electron micrographs of R precipitates for the $[0001]_R$ and $[10\bar{1}0]_R$ electron incidences. Note that the $[10\bar{1}0]_R$ direction is obviously perpendicular to the $[0001]_R$ and $[\bar{1}2\bar{1}0]_R$ directions. Figure 2 shows two high-resolution electron micrographs taken from an equilibrium sample annealed for 24 h, together with two corresponding calculated micrographs. The projections of the R structure along the $[0001]_R$ and $[10\bar{1}0]_R$ directions are also depicted in the insets. The defocus values and the sample thicknesses were estimated to be about -60 nm and about 15 nm for the $[0001]_R$ micrograph in (a) and about -60 nm and about 20 nm for the $[10\bar{1}0]_R$ one in (b). The calculated micrographs in (a′) and (b′) were actually obtained using these values.

In the (a) $[0001]_R$ micrograph, we can see a regular arrangement of bright dots with hexagonal symmetry, whose spacing was determined to be about 0.62 nm. Such an arrangement of dots with hexagonal symmetry is reproduced in the calculated micrograph in (a′). From a comparison with the $[0001]_R$ projection of the R structure, we understand that each bright dot represents a center of an atomic column indicated as the transparent gray hexagon in the projection, although the detailed features of the column in the R structure will be described later. In other words, an array of dots in the micrograph corresponds to that of atomic columns in the R structure.

In the (b) $[10\bar{1}0]_R$ micrograph, on the other hand, bright dots are arranged regularly along the $[0001]_R$ and $[\bar{1}2\bar{1}0]_R$ directions. The calculated $[10\bar{1}0]_R$ micrograph in (b′) also reproduces an array of dots in the experimental one. The axis of the atomic column is obviously parallel to the $[0001]_R$ direction. The point to note here is that, because the R structure involves three types of atomic columns, AC1, AC2, and AC3, the $[10\bar{1}0]_R$ projection consists of the projections of

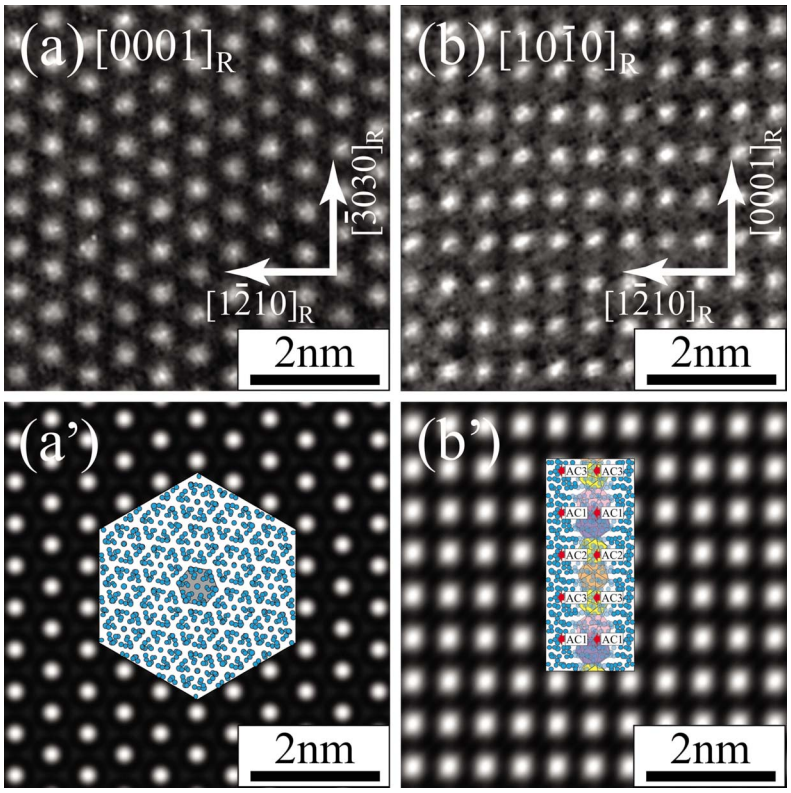

FIG. 2. (Color online) Two high-resolution electron micrographs of an R precipitate in a Fe-18 at. % Mo sample annealed for 24 h, together with corresponding calculated micrographs. The electron incidences of the micrographs in (a) and (b) are, respectively, parallel to the $[0001]_R$ and $[10\bar{1}0]_R$ directions. The computer simulation based on the multi-slice technique was made using $t=15$ nm and $f=-60$ nm for the calculated $[0001]_R$ micrograph in (a′), and $t=20$ nm and $f=-60$ nm for the calculated $[10\bar{1}0]_R$ one in (b′), where t and f denotes the sample thickness and the defocus value. In the calculated micrographs, projections of atomic positions in the R structure are also depicted in the insets. Furthermore, in the projections, one atomic column is denoted by the transparent colored regions, and a CN16-polyhedron pair involved in a column by the transparent pink and purple regions. The details of the correspondence between the colored regions and the polyhedra are shown in Fig. 4.

these three columns. The difference among these three columns is the position of a pair of two CN16 polyhedra in a column. When the distance between two neighboring CN16-polyhedron pairs in a column is taken as unity, the positions of pairs in the three types of columns are characterized by a one-third shift along the $[0001]_R$ column-axis direction. One AC1 column is, for instance, surrounded by three AC2 and three AC3 columns. As a result of the one-third shift, in the $[10\bar{1}0]_R$ micrograph, we can separately detected the projected positions of the CN16-polyhedron pairs in these columns. In the inset of (b′), the array of CN12 polyhedra and CN16-polyhedron pairs in one atomic column, which is here referred to as the AC1 column, is drawn as the transparent colored regions. In addition, the projected-center positions of pairs in these three columns are indicated by the arrows denoted as AC1, AC2, and AC3, respectively. Based on the comparison between the calculated micrograph and the $[10\bar{1}0]_R$ projection, it is thus understood that each dot in the $[10\bar{1}0]_R$ micrograph corresponds to a projected-center position of a CN16-polyhedron pair, here drawn as the transparent pink and purple regions. In other words, we can check the detailed features of an arrangement of CN16-polyhedron pairs in these columns by taking high-resolution electron micrographs for the $[10\bar{1}0]_R$ electron incidence. It is again stressed that an atomic column in the R structure involves CN16-polyhedron pairs, while the column in the μ structure consists of only CN12 polyhedra.[11]

As was mentioned earlier, the initial and intermediate transitional states related to the R-structure formation appeared in samples annealed for 1 and 3 min. In particular, the initial state was mainly found in small precipitates with sizes of less than 10 nm in 1 min annealed samples. Figure 3 shows three pairs of high-resolution electron micrographs of the initial, intermediate, and equilibrium states for the $[111]_{bcc}(\|[0001]_R)$ and $[5\bar{4}\bar{1}]_{bcc}(\|[10\bar{1}0]_R)$ electron incidences. The two pairs for the initial and intermediate states were taken from precipitates of about 9 and about 50 nm in sizes. Note that the micrographs of the equilibrium state are the same as those in Fig. 2. In the (a) $[111]_{bcc}$ micrograph of the initial stage, no-contrast regions are present in the precipitate, and bright dots are observed only in a small region with a size of about 3 nm, as indicated by the arrow. Because each dot corresponds to an atomic column, as pointed out in Fig. 2, columns should first appear locally in the bcc matrix. Hence, there still exist bcc regions in the precipitate, although they should involve local atomic shifts related to the atomic-column formation. On the other hand, we can see an array of bright dots, representing CN16-polyhedron pairs, along the $[0001]_R$ direction in the $[5\bar{4}\bar{1}]_{bcc}$ micrograph in (a′). The inset shows an enlarged micrograph of the area surrounded by the white square in (a′). The notable features of the array of pairs in the projection are that, as indicated by the thick and small arrows in the inset, the spacing between two neighboring projected positions of pairs along a $[0001]_R$ column-axis line is not uniform and that arrays of projected positions in neighboring column-axis lines are basically different from each other. These observations suggest that there is no one-third-shift relationship among neighboring atomic columns, which further implies that atomic columns are nucleated independently in the bcc matrix. It is thus understood that the initial state can be characterized by the local formation of atomic columns in the bcc matrix. In other words, the atomic column is identified as the secondary

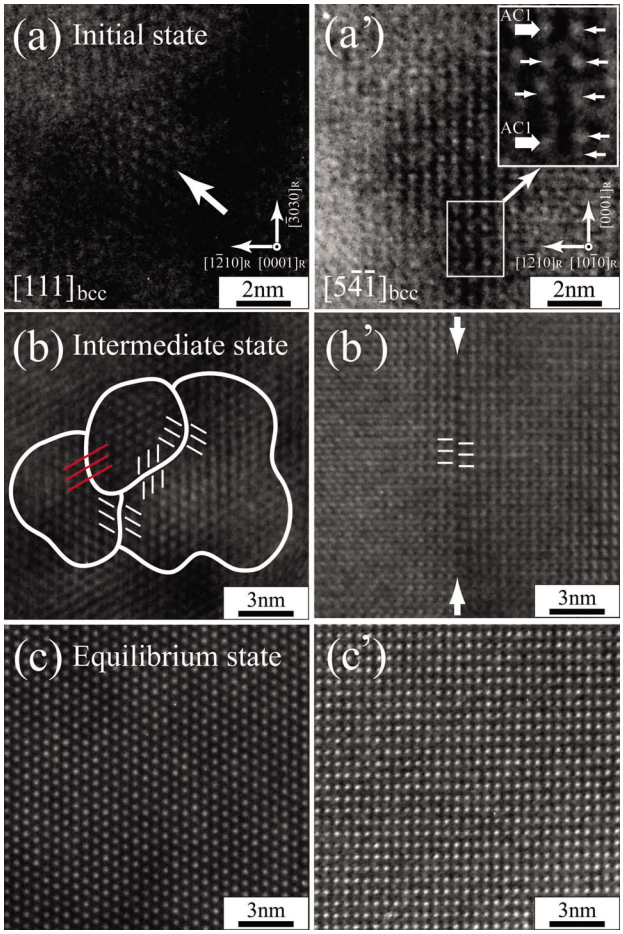

FIG. 3. (Color online) Three pairs of $[0001]_R$ and $[10\bar{1}0]_R$ high-resolution electron micrographs for the initial, intermediate, and equilibrium states appearing during the bcc-to-*R* structural change. In the initial state, bright dots representing atomic columns in (a) can be detected in a small area with a size of about 3 nm, as indicated by the arrow, and atomic columns in (a′) are not developed along the $[0001]_R$ column axis. In particular, an irregular array of CN16-polyhedron pairs is clearly seen, as indicated by the small arrows in the inset of (a′), which shows an enlarged micrograph of the area surrounded by the white square. In the inset, the thick arrows denoted as AC1 indicate projected-center positions of CN16-polyhedron pairs in an AC1 column as a reference. On the other hand, the micrographs in the intermediate state, (b) and (b′), exhibit the presence of a domain structure with an average domain size of about 8 nm, and a hexagonal array of atomic columns, indicating the *R* structure, is seen in the interior of each domain. Based on an array of bright dots, domain boundaries in the domain structure can be identified as out-of-phase boundaries with respect to the arrays of both atomic columns and CN16-polyhedron pairs. The micrographs of the equilibrium state in (c) and (c′) are identical to those in Figs. 2(a) and 2(b), respectively.

structural units in the *R* structure, just as in the case of the μ structure.

To understand the crystallographic features of the intermediate state appearing in the *R*-structure formation, we next focus on the $[111]_{bcc}$ and $[5\bar{4}\bar{1}]_{bcc}$ micrographs, (b) and (b′), of Fig. 3. As seen in the $[111]_{bcc}$ micrograph, the intermediate state consists of domains with an average size of about 8 nm, outlined by the white curved lines. In the interior of each domain, a hexagonal array of dots corresponding to atomic columns is clearly observed. This suggests that, because each domain has the *R* structure, the intermediate state is formed by both the development of atomic-column regions present in the initial state and the conversion of the remaining bcc regions into atomic-column regions. The features of the domain structure are that, in some boundaries between two neighboring domains, there are certain phase shifts with respect to an atomic-column arrangement, as indicated by the white lines, but that no shift occurs in the others, such as indicated by the red lines. We can then look at the $[5\bar{4}\bar{1}]_{bcc}$ micrograph in (b′) to understand the origin of the appearance of a zero-phase-shift boundary. In the $[5\bar{4}\bar{1}]_{bcc}$ micrograph, bright dots corresponding to CN16-polyhedron pairs are regularly arranged along the $[111]_{bcc}(\|[0001]_R)$ and $[12\bar{3}]_{bcc}(\|[\bar{1}2\bar{1}0]_R)$ directions, but there exists a planar defect perpendicular to the $[\bar{1}2\bar{1}0]_R$ direction, indicated by the thick arrows. The feature of this planar defect is that, as marked by the white straight lines, there is a phase shift with respect to an array of dots, indicating the projected-center positions of CN16-polyhedron pairs, along the $[\bar{1}2\bar{1}0]_R$ direction. Based on these features, the domain boundaries in the intermediate state can be identified as out-of-phase boundaries for the arrays of both atomic columns and CN16-polyhedron pairs. Because the *R* state is characterized by uniform arrangements of both columns and pairs, as seen in the micrographs of the equilibrium state, (c) and (c′), it is therefore clear that the formation of the equilibrium *R* structure from the intermediate state is directly associated with the annihilation of these out-of-phase boundaries.

IV. DISCUSSION

Based on our experimental data, it was found that the *R* structure was formed from the bcc structure via two transitional states. These initial and intermediate states are characterized, respectively, by the nucleation of atomic-column regions in the bcc matrix and the formation of a domain structure consisting of nanometer-sized *R*-structure domains. The interesting feature of the domain structure in the intermediate state is that, at the domain boundaries, there exist certain phase shifts with respect to the arrays of both atomic columns and CN16-polyhedron pairs. These experimental data reveal that atomic columns involving CN16-polyhedron pairs appear first in the bcc-to-*R* structural change. In other words, this is experimental evidence that the atomic column is the secondary structural unit of the *R* structure. With the help of the structural data for the *R* structure in the Mo-Co-Cr alloy system,[10] we here discuss the crystallographic relation between the bcc structure and the atomic column and propose a model of an atomic displacement from the bcc structure for the formation of the CN12 and CN16 polyhedra in the column. Based on the atomic-displacement model, we further try to identify the primary structural unit involved in the atomic column as the secondary structural unit.

Our discussion starts with the structural relation between the bcc and *R* structures. Our experimental data confirmed

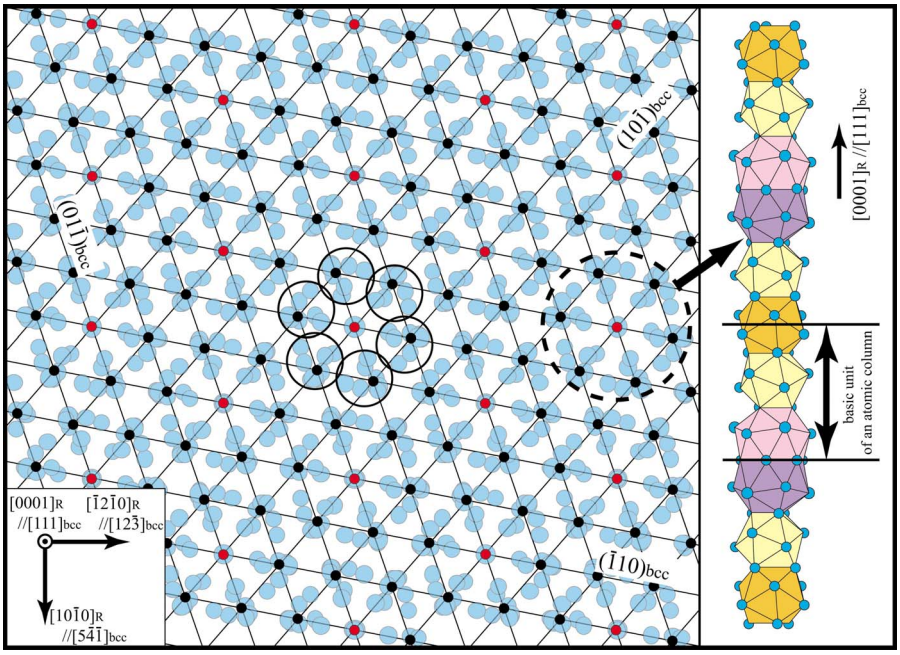

FIG. 4. (Color online) Schematic diagram showing the correspondence between the $[0001]_R$ projected positions of atoms in the R structure and the traces of the $(\bar{1}10)_{bcc}$, $(10\bar{1})_{bcc}$ and $(01\bar{1})_{bcc}$ planes in the bcc lattice. The correspondence shown here is based on the experimentally obtained relations of $[111]_{bcc}\|[0001]_R$ and $(12\bar{3})_{bcc}\|(\bar{7}14\bar{7}0)_R$. The reported structural data of the R structure for the Mo-Co-Cr ternary alloy system are adopted in the diagram (Ref. 10). An atomic column present inside the large dashed circle is also depicted in the inset. Each red cross point of the $\{110\}_{bcc}$ planes is coincident with a position of a column-center axis. Around a black point, the projected positions inside the small solid circles are in the same configuration. In addition, a basic unit of an atomic column, indicated by the double arrow in the inset, consists of a half of an orange CN12, one yellow CN12, and one pink CN16 polyhedra. The basic unit is a repetition of one atomic column and is one-half of a region between two neighboring CN16-polyhedron pairs.

that there was the unique orientation relationship of $[111]_{bcc}\|[0001]_R$ and $(12\bar{3})_{bcc}\|(\bar{7}14\bar{7}0)_R$. Based on this relation, we first draw the $[0001]_R$ projection of the R structure and the bcc lattice together. The traces of the $(10\bar{1})_{bcc}$, $(01\bar{1})_{bcc}$, and $(\bar{1}10)_{bcc}$ planes as well as the projection of the atomic positions in the R structure are depicted in Fig. 4 using the bcc lattice parameter $a=0.292$ nm and the R-structure parameters $a=1.09$ nm and $c=1.92$ nm. Note that these lattice parameters were determined from the analysis of the diffraction patterns in Fig. 1 and that the determined R-structure parameters are almost the same as those reported in the Mo-Co-Cr system, $a=1.0903$ nm and $c=1.9342$ nm.[10] The latter agreement is, in fact, the reason why we used the structural data for the Mo-Co-Cr system to aid this analysis. In addition, as the constituent atoms in the Mo-Co-Cr system are obviously different from those in the Fe-Mo system, it was assumed that the R structure consisted of identical atoms. That is, we paid attention only to the atomic positions and checked the positional relation between the projected positions and the cross points of the $\{110\}_{bcc}$ traces in Fig. 4. The interesting features to be found in this diagram are that the projected positions of atoms present along a column-center axis coincide with the red cross points and that atoms around every black point, indicated by the small circles, are in the same atomic configuration. This implies that, to understand the R-structure formation from the bcc structure, we can focus on only atomic shifts in one atomic column as the secondary structural unit of the R structure. The three-dimensional arrangement of atoms in an atomic column is then depicted in the inset. From this schematic diagram, it is confirmed that the atomic column in the R structure consists of both CN12-polyhedra and CN16-polyhedron pairs. That is, either a CN12 or CN16 polyhedron should be identified as the primary structural unit of the R structure.

Let us here discuss the crystallographic relation between the atomic column and the bcc structure. According to the obtained relationship, the $[111]_{bcc}$ direction is parallel to the $[0001]_R$ column axis. More precisely, in the $[5\bar{4}\bar{1}]_{bcc}$ diffraction pattern [Fig. 1(c)], the location of the 222_{bcc} reflection is almost identical to that of the 00024_R reflection, but the spacing of the $(00024)_R$ plane is about 3.1% shorter than that of the $(222)_{bcc}$ plane. Taking this lattice distortion into account, in Fig. 5, we compare the positions of atoms in the atomic column with the array of the contracted $(222)_{bcc}$ layers with a spacing of about 0.082 nm. It should be remarked that, in the $(222)_{bcc}$ plane of the bcc structure, there are three types of the $(222)_{bcc}$ layers here called the A, B, and C layers. Among these layers, one atom present in each A layer is assumed to sit on the column-axis position. As can be understood from the diagram, atoms in the atomic column are located in layers indicated by the red lines, which are produced by shifts of the contracted $(222)_{bcc}$ layers along the column axis. The notable features found in the diagram are that the A_1 layers are absent in the column because of the

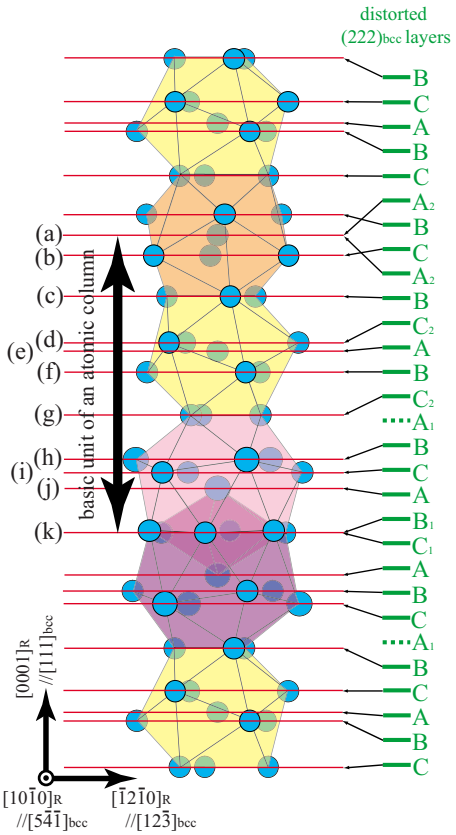

FIG. 5. (Color online) Schematic diagram showing the correspondence between the $[10\bar{1}0]_R$ projection of atomic positions in an atomic column and the $(222)_{bcc}$ layers in the distorted bcc lattice. In the construction of the diagram, we took into account a lattice distortion found in the diffraction patterns of Fig. 1(c). That is, the spacing of the distorted $(222)_{bcc}$ layers in the right side is about 3.1% shorter than that of the $(222)_{bcc}$ plane. Atoms in the column sit on the layers, indicated by the red lines, which are produced by shifts of the distorted $(222)_{bcc}$ layers. A notable feature is that the collapse of two A_2 layers and of the B_1 and C_1 layers as well as the absence of two A_1 layers take place during the formation of an atomic column.

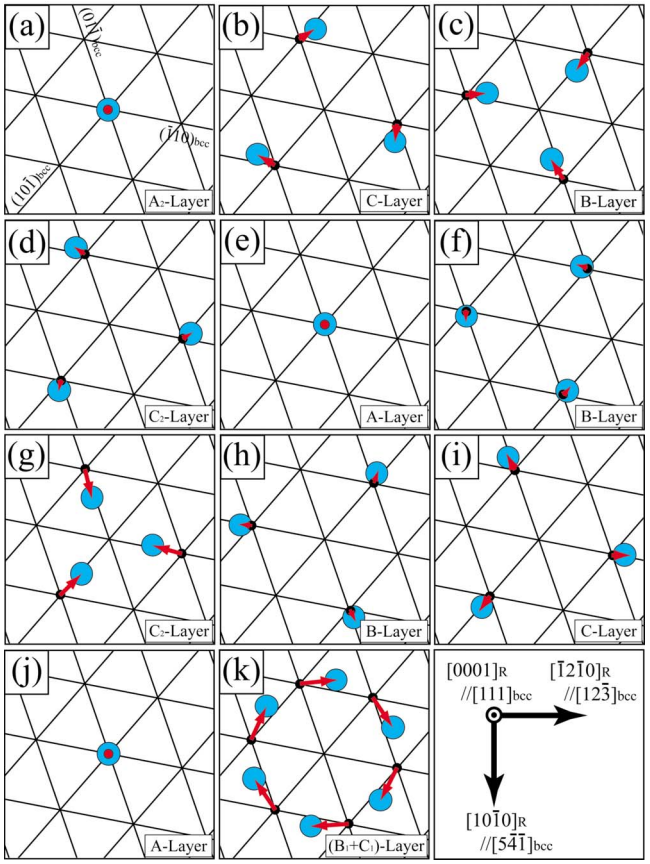

FIG. 6. (Color online) Schematic diagram of atomic-shift components perpendicular to a column-axis direction in the formation of a column from the distorted bcc structure. Atomic positions in the (a)–(k) layers in Fig. 5 and the traces of the $(\bar{1}10)_{bcc}$, $(01\bar{1})_{bcc}$, and $(10\bar{1})_{bcc}$ planes are depicted in the diagram. Atoms in the A and A_2 layers sit on the red cross points: that is, a position of a column axis. Relatively, larger shifts of atoms occur in the lower C_2 and (B_1+C_1) layers.

introduction of vacancies and that two A_2 layers combine into a single layer, denoted by (a) in the column, through the introduction of one vacancy and a layer shift along the column axis. In addition, the (k) layer in the column is produced by the collapse of the B_1 and C_1 layers in the distorted bcc structure. Interestingly, in other words, there is a one-to-one correspondence between the atomic layers in the column and the contracted $(222)_{bcc}$ layers. This correspondence clearly indicates that the atomic positions in the column of the *R* structure can be produced from those in the distorted bcc structure by simple atomic shifts.

To understand the detailed features of atomic-shift components perpendicular to the column axis, the locations of atoms in the (a)–(k) layers in Fig. 5 are depicted in Fig. 6, together with the traces of the $\{110\}_{bcc}$ planes. In the diagram, we show only atomic shifts for a basic unit of an atomic column, which is defined as one-half of a region between two neighboring CN16-polyhedron pairs in a column. This is because the basic unit is a repetition of one atomic column. It is found that atomic shifts in almost layers are very simple and small and that relatively large shifts occur only in the (g) and (k) layers. Even in these two layers, however, we can easily assign a cross point for each atom. Therefore, the one-to-one correspondence is also established between each atomic position in a column and a distorted bcc lattice point.

The atomic column in the *R* structure, as the secondary structural unit, consists of CN16 and CN12 polyhedra, as shown in Fig. 4. Based on the presence of the above-mentioned one-to-one correspondence, we propose an atomic-displacement model for the formation of these polyhedra from the distorted bcc structure. Before displaying these displacements, we have to point out that there are two kinds of CN12 polyhedra in the atomic column. The important point to note here is that, as shown in the diagrams in Figs. 5 and 6, the atomic shifts in one CN12 polyhedron are entirely different from those in the other. That is, there are two types of atomic displacements for the formation of the CN12 polyhedron in the bcc-to-*R* structural change. Based

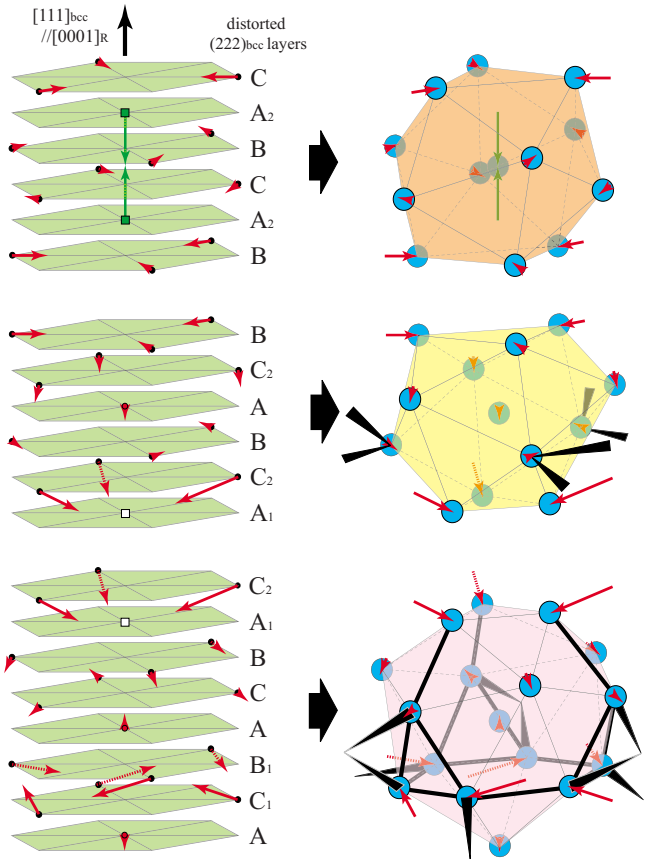

FIG. 7. (Color online) Three-dimensional schematic diagram showing atomic shifts for the formation of the CN12 and CN16 polyhedra involved in an atomic column of the *R* structure. In the diagram, lattice points in the distorted $(222)_{bcc}$ layers before atomic shifts indicated by the red arrows are depicted in the left side, while the right-side diagram shows the atomic positions in two CN12 and one CN16 polyhedra formed after the shifts. The notable features before the shifts are that there are vacancies marked by the open squares in the A_1 layers and that one vacancy should be present at one of the two green squares in the A_2 layers. One atom left in the A_2 layers is shifted along the green arrow. Further, in the right diagram, the thick black lines and the black elongated triangles indicate bonds shorter than 0.237 nm, which are produced by the large atomic shifts. These shorter bonds should have a covalent-bond character.

on this fact, these two types of atomic displacements as well as the displacement for the CN16 polyhedron are schematically shown in Fig. 7; this figure also shows atomic bonds that are shorter than 0.237 nm, indicated by both the thick black lines and the black elongated triangles.[10] We first focus on two types of displacements for the formation of a CN12 polyhedron. One displacement shown in the upper diagram is mainly characterized by both the introduction of one vacancy in two A_2 layers and a relatively large shift along a column axis for an atom left in one of the layers. For the other displacement depicted in the middle, the absence of the A_1 layer, which is caused by the introduction of a vacancy, results in very large shifts of three atoms in the lower C_2 layer. As for the CN16 polyhedron in the lower diagram, the polyhedron is formed not only by the very large shifts of the atoms in the C_2 layer but also by the markedly very large shifts of six atoms associated with the collapse of the B_1 and C_1 layers. The most important point found in the diagrams is that these quite large and very large shifts result in the shorter bonds indicated by both the thick black lines and the black elongated triangles. Among these shorter bonds, those indicated by the thick black lines are involved only in the CN16 polyhedron, while the others shown as black elongated triangles play the role of bonds connecting two neighboring columns. The shortest bond with a length of about 0.227 nm is obviously involved in a CN16 polyhedron, and there is no shorter bond found in the two kinds of CN12 polyhedra. Based on the presence of the shorter bonds in the CN16 polyhedron, it is probably that the primary structural unit of the *R* structure is a CN16 polyhedron, instead of a CN12 one, as found in the case of the μ structure.[11]

We finally discuss the origin of the appearance of the CN16 polyhedron with shorter bonds as the primary structural unit of the *R* structure. As was mentioned above, the shorter bonds are produced by the large atomic shifts associated with the introduction of a vacancy and the collapse of two layers in the distorted bcc structure. We then estimate the reduction percent of a bond length in the bcc-to-*R* structural change. For the bcc lattice with a parameter $a=0.292$ nm, the shortest bonds along the $\langle 111\rangle_{bcc}$ directions have a length of about 0.253 nm. A reduction in bond lengths from 0.253 to 0.237 nm is then calculated to be $100\times(0.253-0.237)/0.253\sim 6.3\%$. Of particular note is that the shortest 0.227 nm bond in the *R* structure is reduced by a surprising 10.3%. This large reduction suggests that the shorter bonds in the *R* structure have a covalent character, just like atomic bonds forming CN12 polyhedra in the Laves and μ structures.[11,14–16] In other words, the appearance of the CN16 polyhedron in the atomic column is associated with the formation of covalent bonds in transition-metal alloys. In addition, it is likely that the formation of covalent bonds in the CN16 polyhedron may attribute to the stability of the *R* structure, presumably via an opening of a band gap or pseudo gap at the Fermi level E_F. The presence of such a gap induced by hybridization has recently been discussed in relation to the stability of crystal structures in alloys, such as Al-based icosahedral quasicrystalline approximant crystals and the triclinic Al_2Fe phase.[17–19] Although defining the details of the relationship between the formation of covalent bonds in a CN16 polyhedron and the stability of the *R* structure is a task for the future, the *R* structure is believed to be the example where the CN16 polyhedron can be identified as the primary structural unit of an alloy crystal structure.

V. CONCLUSIONS

The experimental results present here revealed that the bcc-to-*R* structural change occurred via initial and intermediate transitional states. In the initial stage, atomic columns consisting of both CN12-polyhedra and CN16-polyhedron pairs were first formed independently. The orientation relationship obtained between the bcc and *R* structures indicated that the CN12 and CN16 polyhedra in an atomic column could be formed by the introduction of both atomic vacan-

cies and simple atomic shifts. That is, the introduction of vacancies plays an essential role in the atomic-column formation in the *R* structure, while no vacancy is needed for the μ-structure column consisting of only CN12 polyhedra. In addition, the atomic shifts in the bcc-to-*R* structural change result in the formation of a CN16 polyhedron with shorter bonds as the primary structural unit of the *R* structure. The shorter bonds should have a covalent character. The appearance of the CN16 polyhedron with shorter bonds in the *R* structure must be directly associated with the formation of covalent bonds in transition-metal alloys.

ACKNOWLEDGMENT

This work was partially supported by the Ministry of Education, Science, Sports and Culture, Grant-in-Aid for Scientific Research (B), Japan (No. 18360306) 2007.

[1] P. I. Kripyakevich, Sov. Phys. Crystallogr. **5**, 69 (1960).
[2] P. I. Kripyakevich, *A Systematic Classification of Types of Intermetallic Structures* (Consultants Bureau, New York, 1964).
[3] K. Schubert, *Kristallstrukturen Zweikomponentiger Phasen* (Springer-Verlag, Berlin, 1964).
[4] W. B. Pearson, in *Developments in the Structural Chemistry of Alloy Phases*, edited by B. C. Giessen (Plenum, New York, 1969).
[5] W. B. Pearson, *The Crystal Chemistry and Physics of Metals and Alloys* (Wiley, New York, 1972).
[6] S. Samson, in *Structural Chemistry and Molecular Biology*, edited by A. Rich and N. Davidson (Freeman, San Francisco, 1969).
[7] J. B. Forsyth and L. M. D'Alte Da Veiga, Acta Crystallogr. **15**, 543 (1962).
[8] A. K. Sinha, R. A. Buckley, and W. Hume-Rothery, J. Iron Steel Inst., London **205**, 191 (1967).
[9] C. B. Shoemaker and D. P. Shoemaker, Acta Crystallogr., Sect. B: Struct. Crystallogr. Cryst. Chem. **34**, 701 (1978).
[10] Y. Komura, W. William, and D. Shoemaker, Acta Crystallogr. **13**, 575 (1960).
[11] A. Hirata, A. Iwai, and Y. Koyama, Phys. Rev. B **74**, 054204 (2006).
[12] C. P. Heijwegen and G. D. Rieck, J. Less-Common Met. **37**, 115 (1974).
[13] P. Donnadieu and A. Redjaimia, Philos. Mag. B **67**, 569 (1993).
[14] Y. Kubota, M. Takata, M. Sakata, T. Ohba, K. Kifune, and T. Tadaki, J. Phys.: Condens. Matter **12**, 1253 (2000).
[15] A. Hirata, Y. Koyama, and M. Tanimura, Phys. Rev. B **67**, 144107 (2003).
[16] A. Hirata and Y. Koyama, Phys. Rev. B **70**, 134203 (2004).
[17] M. Weinert and R. E. Watson, Phys. Rev. B **58**, 9732 (1998).
[18] K. Kirihara, T. Nakata, M. Takata, Y. Kubota, E. Nishibori, K. Kimura, and M. Sakata, Phys. Rev. Lett. **85**, 3468 (2000).
[19] M. Krajčí and J. Hafner, J. Phys.: Condens. Matter **14**, 5755 (2002).